11A-02

INTERCOMPARIONS OF CLOUDSAT AND GROUND-BASED RADAR MEASUREMENTS DURING SATELLITE OVERPASSES

Sergey Y. Matrosov[1], A. V. Ryzhkov[2], J. Hardin[3], M. D. Shupe[1], M. Maahn[1], G. de Boer[1], and T. Uttal[4]

[1]Cooperative Institute for Research in Environmental Sciences,
University of Colorado and NOAA ESRL, Boulder, Colorado
[2] Cooperative Institute for Mesoscale Meteorological Studies
University of Oklahoma and NOAA NSSL, Norman, Oklahoma
[3] Pacific Northwest National Laboratory, Richland, Washington
[4]NOAA Earth System Research Laboratory, Boulder, Colorado

1. INTRODUCTION

The CloudSat satellite, which carries a nadir - pointing W-band cloud profiling radar (CPR), passes over a number of ground-based operational and research radars. Close time and 3D space collocations of satellite and ground-based radar measurements are possible during the overpasses. Due to excellent calibration of the CPR, collocated measurements can be used for the relative calibration of the ground-based radars and also for intercomparisons of the microphysical retrievals for matched vertical profiles. Matched profile intercomparisons largely avoid uncertainties associated with different space averaging of gridded satellite and ground-based radar products thus allowing for detailed evaluation of the retrieval algorithms and better understanding of their uncertainties.

The focus of this study is on retrieval results of such precipitating ice microphysical parameters as hydrometeor characteristic size and ice/snow water content. The data sets used in this study were collected during CloudSat overpasses near the Oliktok Point, Alaska Atmospheric Radiation Measurement (ARM) program's Mobile Facility 3 (AMF3) and several operational Weather Surveillance Radar-1988 Doppler (WSR-88D) S-band units in the continental USA.

2. INTERCOMPARISONS DURING OLIKTOK POINT OVERPASSES

A dual-frequency (K_a- and W-band, 35 GHz and 94 GHz) fully polarimetric scanning ARM radar (SACR) was deployed at AMF3 in 2016-2017. At that time the CloudSat satellite was part of the polar orbiting A-train satellite constellation, which was passing over the vicinity of the AMF3 every 16 days. During several months in 2017, a special SACR scanning mode was executed during overpasses to better match the SACR and CloudSat radar measurements. This procedure included a range-height indicator (RHI) scans parallel to the CloudSat ground track (at a 26.3° azimuth) about 1.5 min prior and 1.5 min after the CloudSat passage and an RHI scan perpendicular to the satellite track at the time of passage (at a 116.3° azimuth).

Corresponding author address: Sergey Matrosov, R/PSDN, 325 Broadway, Boulder, CO 80305, email: sergey.matrosov@noaa.gov

Figure 1 shows a map depicting CloudSat overpasses over Oliktok facility on three different occasions when both the CPR and the SACR were observing clouds and precipitating hydrometeors. For all these overpasses the CloudSat crossed over the vicinity of the AMF3 located at N70.495°, W149.866°. at about 13:21 UTC on a descending satellite orbit.

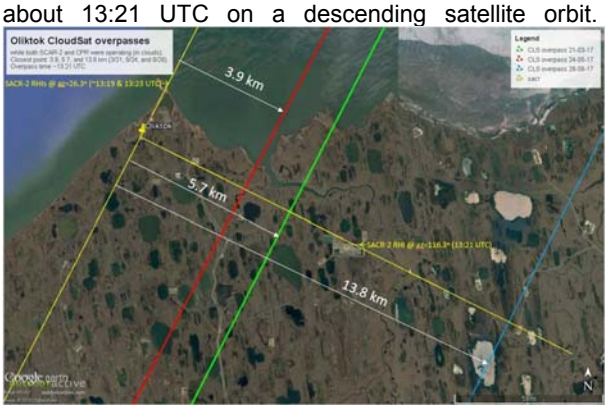

FIG.1. *Center beam CPR ground tracks during the overpasses on 21 March (green), 24 May (red) and 28 August (blue). Yellow lines show SACR RHIs parallel and perpendicular to the CloudSat ground tracks. Distances from the AMF3 and the center of the CPR footprint are in white.*

The closest to the AMF3 CloudSat overpass occurred on 24 May 2017 during a light snowfall event. Figure 2 shows CPR and SACR reflectivity cross sections during this overpass. The SACR sensitivity in a scanning mode was too low to reliably measure low reflectivity radar echoes near cloud boundaries and even in the middle of the cloud at low signal-to-noise ratios (SNRs) when viewing at slant distances beyond 10 km or so. Otherwise, in the regions of larger SNRs, there is a general agreement between CPR and SACR measurements. According to the AMF3 radiosonde soundings (not shown), temperatures in the entire atmospheric columns were below the freezing point, so no precipitating liquid hydrometeors were expected. Microwave radiometer based retrievals of liquid water path (LWP) during this overpass were around 40 g m^{-2} indicating presence of only relatively small amounts of supercooled cloud liquid.

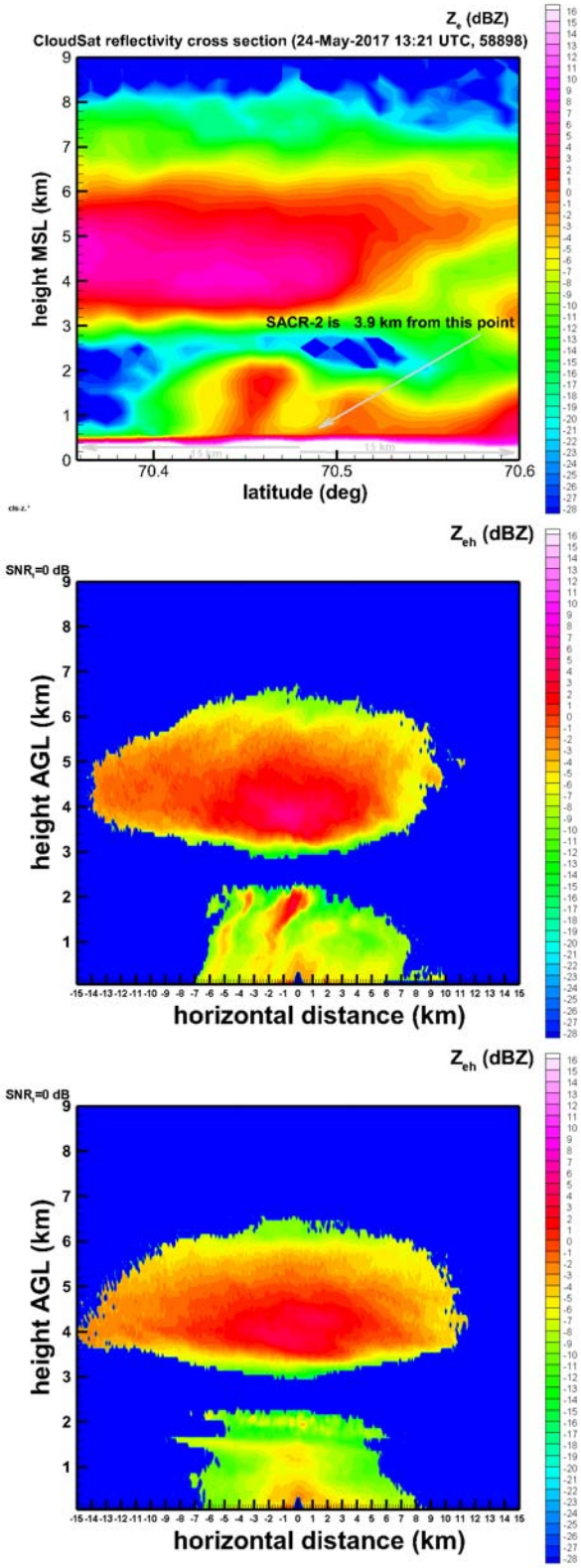

FIG.2. *W-band reflectivity cross-sections from CloudSat CPR at 13:21 UTC 24-May 2017 (upper frame) and the SACR parallel (at ~13:23 UTC, middle frame) and perpendicular (at ~ 13:21 UTC, lower frame) to the satellite ground track.*

2.1 *CPR and SACR reflectivity comparisons*

Figure 3 shows comparisons of the W-band CPR and SACR reflectivity profile measurements during the 24 May 2017 overpass. The SACR reflectivity profiles are shown for two points: (*a*) a true vertical profile at the AMF3 location (70.495ºN, 149.886ºW), and (*b*) for a point corresponding to center of the CloudSat pixel, which was the closest (~3.9 km) to the AMF3 (70.479ºN, 149.792ºW). These vertical profiles were reconstructed from the SACR 116.3º azimuth RHI scan at 13:21 UTC. When reconstructing the profile (*b*) from off zenith RHI measurements, the SACR data were overaged over 1.5 km horizontal distance interval (i.e., the CPR cross track pixel size) to mitigate effects of differing fields of views of ground-based and satellite radar measurements. The CPR profile in Fig. 3 was taken near the location closest to the AMF3.

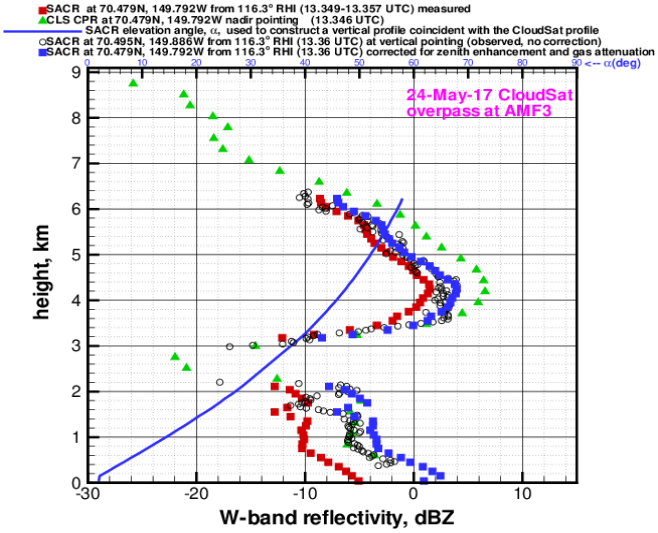

FIG.3. *Profiles of reflectivity during the 24-May-2017 overpass. CPR profile corrected for gaseous attenuation (green), the observed SACR profile at zenith (black), the observed SACR profile matched with the CPR measurements (red) and the SACR profile matched with the CPR data and corrected for gaseous attenuation and zenith enhancements (blue symbols). The blue line shows SACR elevation angles used for reconstructing the profile matched with CPR data.*

Since the SACR reflectivities matched with satellite measurements were collected at slant viewing, they need to be corrected for the zenith enhancement. This enhancement is present for larger non-spherical particles for which scattering is outside the Rayleigh scattering regime (e.g., Matrosov et al. 2012). Particles with a greater degree of non-sphericity cause stronger zenith reflectivity enhancements. The enhancement corrections were derived from the elevation angle dependencies of SACR reflectivities assuming that for the relatively short radar ranges considered here for comparisons, the horizontal layers of hydrometeors are reasonably homogenous. Note that CPR multiple scattering effects are partially compensated by snow attenuation (e.g., Matrosov and Battaglia 2009).

Figure 4 shows elevation angle dependencies of SACR W-band reflectivities at various constant altitudes. An approximate symmetry of the curves relative to the zenith direction is expected from horizontally homogeneous layers of hydrometeors. It can be seen from Fig. 4 that the zenith reflectivity enhancements are altitude dependent (e.g., enhancements are practically negligible in the higher regions of the upper cloud echo).

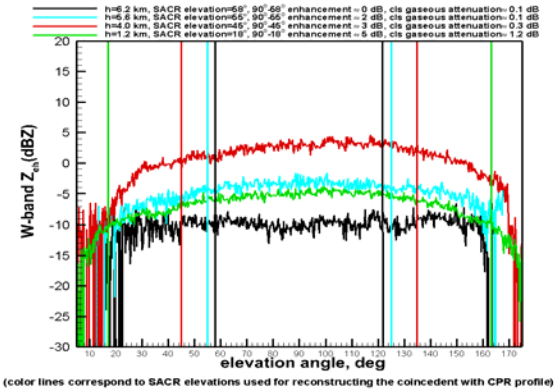

FIG.4. *Constant altitude elevation angle dependencies of SACR reflectivities (from the 116.6º azimuth RHI at 1321UTC on 24-May-2017). Green, red, cyan and black curves correspond to altitudes of 1.2, 4.0, 5.6, 6.2 km.*

SACR zenith reflectivity corrections at different altitudes were estimated at elevation angles used for reconstructing the SACR vertical profile matched with the CPR profile. Overall these corrections were on the order of several dB. Such enhancement are expected from moderately non-spherical particles. The presence of such particles is evident from the SACR differential reflectivity, Z_{DR}, RHI data, which are shown in Fig. 5.

As seen from Fig.3, closely collocated CPR and corrected SACR reflectivities generally agree within about ±2 dB (blue and green symbols). Since the CPR is well calibrated using the ocean scatter reference technique, this agreement provides confidence in the absolute calibration of SACR reflectivities.

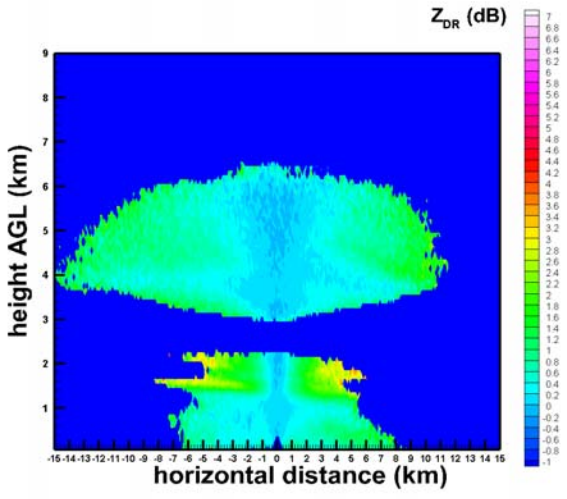

FIG.5. *SACR Z_{DR} for the 116.6º RHI (13:21UTC).*

2.2 *Microphysical retrieval comparisons*

For the CPR and SACR collocated radar reflectivity profiles, Fig.6 depicts retrievals of ice water content (IWC). Satellite-based IWC data are shown for retrievals from the two standard CloudSat algorithms (2C-SNOW-PROFILE and 2B-CWC-RO data available at http://www.cloudsat.cira.colostate.edu/data-products). The standard version of the latter algorithm assumes temperature dependent cloud content partitioning between liquid and solid state. However, since reflectivities were dominated by ice particles during the overpass, results from this algorithm are also shown assuming ice only scatterers (i.e., 2B-CWC-RO/IO). Satellite retrievals are not available at lower altitude (less than about 1 km) due to potential contamination of hydrometeor reflectivity data by ground clutter.

Ground-based retrievals were performed using the cloud-radar based algorithm described by Shupe et al. (2005). Since this algorithm was developed for the K_a-band radar data, retrievals were performed using the K_a-band SACR measurements. It did not affect the spatiotemporal collocation of ground-based and satellite measurements because W- and K_a-band SACR beams are matched. Uncertainties of ground based retrievals due to ±1 dB errors in the SACR absolute calibration are also shown in Fig. 6 (*cyan curves)*. Note that the zenith reflectivity enhancement effects for the K_a-band measurements were negligible (not shown).

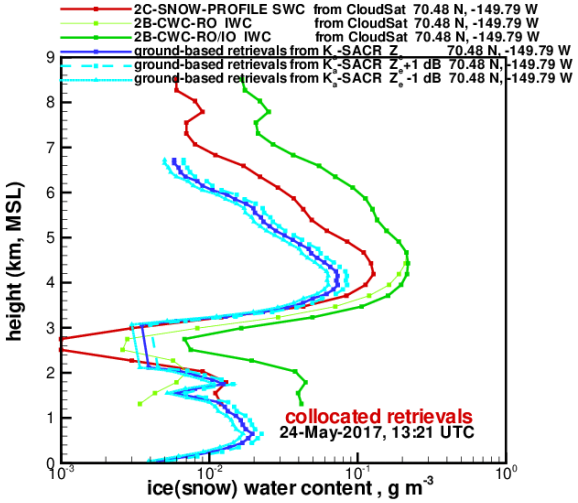

FIG.6. *Comparisons of collocated CloudSat (red and green curve) and SACR (blue curve) retrievals of IWC at the AMF3 location.*

As seen from Fig. 6, there are significant discrepancies in the IWC retrieval results from various algorithms. For the upper cloud, IWC differences could be greater than a factor of 3. Even different CloudSat algorithms provide retrievals which differ as much of the factor of 3 even though they use exactly the same CPR reflectivity measurements as the input information. These differences are primarily due to differing *a priori* assumptions (e.g., Matrosov 2019).

Figure 7 shows matched intercomparisons of the characteristic particle size. Different algorithms retrieve

different sizes that characterize the entire particle size distribution (PSD). The CloudSat algorithms retrieve the exponential slope Λ of the exponential distribution (2C-SNOW-PROFILE) and the effective particle diameter, D_e, representing the ratio of the third and second PSD moments (2B-CWC-RO). The ground-based radar algorithm retrieves mean particle size D_{mean} (i.e., the ratio of the first and zeroth PSD moments). In order to provide meaningful comparisons, all the retrievals results were recalculated to the median volume particle size D_{mv}, given in terms of the major particle dimension.

In order to find mean statistical relations between different characteristic sizes they were calculated for the large number of *in situ* PSDs observed during the Indirect and Semi-Direct Aerosol Campaign (ISDAC) in Alaska (Maahn 2015). According to these calculations the mean values for the D_e/D_{mv} ratio was 0.92. This value was further used for converting 2B-CWC-RO algorithm particle size retrievals to D_{mv}. The exponential slope from the 2C-SNOW-PROFILE algorithm is related to D_{mv} as D_{mv}=3.67/Λ. The mean size from the ground-based retrievals was converted to D_{mv} assuming the exponential PSD as D_{mv}=3.67D_{mean}.

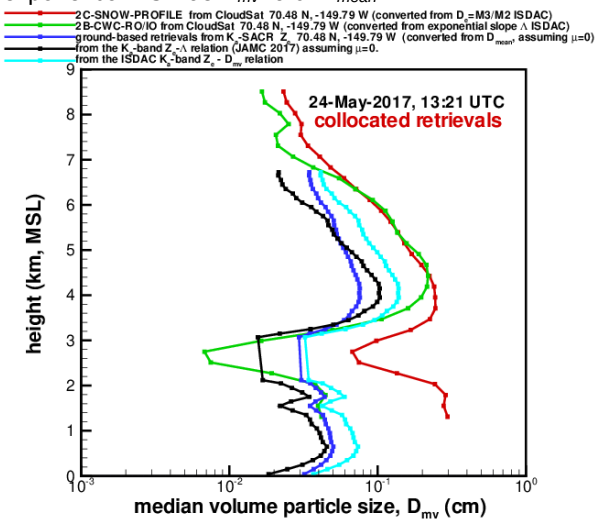

FIG.7. *Collocated retrievals of median volume particle size. CloudSat retrievals are in red (2C-SNOW-PROFILE) and green (2B-CWC-RO/IO), ARM ground-based retrievals are in blue. Black and cyan curves show size estimates using reflectivity – size relations.*

In addition to the standards CloudSat 2C-SNOW-PROFILE and 2B-CWC-RO/IO retrievals, Fig. 7 shows retrievals based on statistical relations between radar reflectivity and particle characteristic size. The black curve shows retrievals using K_a-band reflectivity – characteristic size parameter relation from (Matrosov and Heymsfield 2017), assuming the exponential PSD type, and the cyan curve depicts the results from applying the statistical relation between reflectivity and D_{mv} found from ISDAC *in situ* data: D_{mv}(cm)=0.12 $Ze^{0.29}$, where K_a-band Z_e is in mm^6m^{-3}.

As for IWC retrievals, differences in characteristic particle size retrievals using different algorithms are as large as a factor 3, although they are smaller in a lower part of the radar echo (excluding 2C-SNOW-PROFILE retrievals). Interestingly, the size estimates based on simple statistical D_{mv} - Z_e relations are overall in fair agreement with the results (given a general data scatter) of more sophisticated satellite and ground-based algorithms.

3. INTERCOMPARISONS DURING WSR-88D SITES OVERPASSES

The CloudSat satellite also regularly passes over the vicinity of several WSR-88D sites. During such overpasses, it is possible to closely match CPR and WSR-88D measurements in time and space with approximate accounting for differing radar resolutions (Matrosov 2019). An example of one such collocation is shown in Fig. 8. It corresponds to a CloudSat overpass over the vicinity of the WSR-88D unit (a four-letter unit identifier is KMQT) during a snowfall event. All temperatures were below the freezing point thus no bright band effects were expected (e.g., Sassen et al. 2007). The KMQT site is located near Marquette, MI at N46.531°, W87.548°. The cross section of ground-based measurements along the CloudSat ground track was compiled from the KMQT volume scan data.

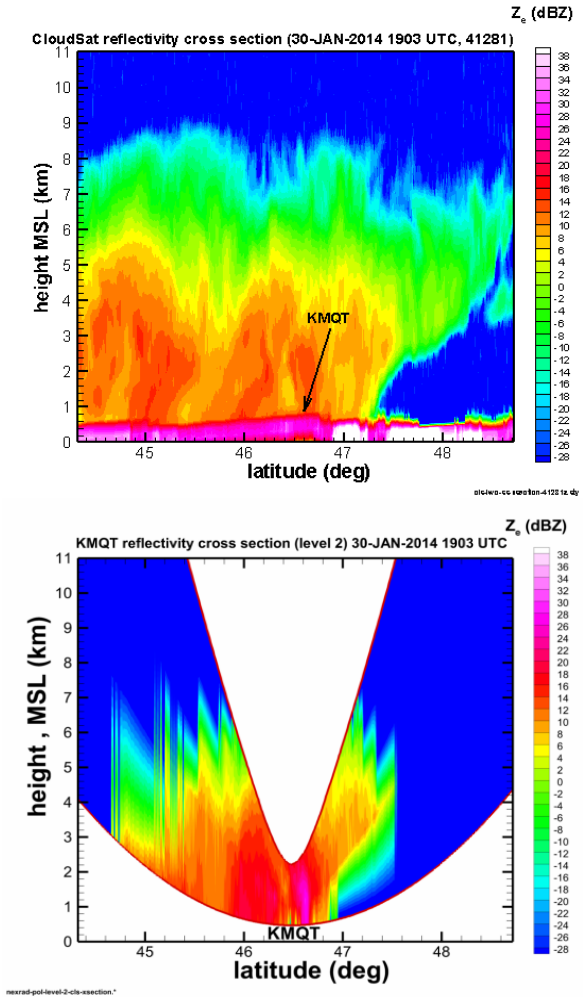

FIG.8. *Matched CPR (upper frame) and KMQT (lower frame) reflectivity data on 30-JAN- 2014 (1903 UTC).*

Due to the Earth sphericity, the KMQT radar does not have observations near the ground up to a certain altitude which becomes progressively higher with range. Regions above the radar also lack observations due to the absence of WSR-88D data at higher elevation angles. Despite these limitations, the region of overlapping ground-based and satellite measurements is large enough for meaningful intercomparisons.

Figure 9 shows intercomparisons of particle size retrievals. Besides CloudSat retrievals using its standard algorithms, three types of WSR-88D based estimates are also shown. The two types are based on polarimetric measurements. The first polarimetric estimator uses specific differential phase shift K_{DP} (in deg km^{-1}) and horizontal polarization reflectivity Z_e, (the black curve in Fig. 9) and the second one (the blue curve in Fig.9), which is less susceptible to variability in particle shape and orientations, uses the Z_{DP} / K_{DP} ratio (Ryzhkov et al. 2018) where Z_{DP} is the difference between horizontal and vertical polarization reflectivities (in mm^{6}m^{-3}). A relatively stable particle size retrievals from polarimetric data are available when K_{DP} values exceed about 0.05 deg km^{-1}. The polarimetric measurements were derived using the quasi vertical profile (QVP) methodology (Ryzhkov et al. 2018).

The third WSR-88D based estimator of particle characteristic size uses an S-band statistical relation between D_{mv} and Z_e. This relation was found from *in situ* ISDAC measurements and is shown in Fig. 10. Details of reflectivity calculations from *in situ* measurements are given by Maahn et al. (2015). The ISDAC data set was also used to find average correspondences between median volume particle size, D_{mv}, and other characteristic PSD sizes used in the literature, such as the mean volume size, D_m, the effective size, D_e, and the mean size D_{mean}, which represent the ratios of the forth and the third PSD moments (for D_m), the third and the second PSD moments (for D_e), and the first and the zeroth PSD moments (for D_{mean}): $D_m/D_{mv} \approx 1.09$, $D_e/D_{mv} \approx 0.92$, and $D_e \approx 0.0348\ D_{mv}^{0.616}$ (where D_{mv} is in meters).

As seen from Fig. 9, polarimetric WSR-88D retrievals indicate generally smaller particle sizes (especially in the upper part of the precipitating cloud) compared with satellite retrievals and reflectivity only based KMQT estimates. As with intercomparisons of SACR and CloudSat retrievals above Oliktok Point the differences in particle characteristic size estimates from different retrieval algorithms can exceed a factor of 2.

Figure 11 shows intercomparisons of KMQT and CloudSat-based retrievals of IWC. Depicted ground-based retrievals include polarimetric estimates based on QVPs of K_{DP} and differential reflectivity, Z_{DR}, and collocated with the CPR data estimates based on applying IWC-Z_e – temperature statistical regressions from Hogan et al. (2006). Besides the standard algorithm results, the CloudSat retrievals include also estimates based on the IWC – reflectivity regression (Matrosov and Heymsfield 2008).

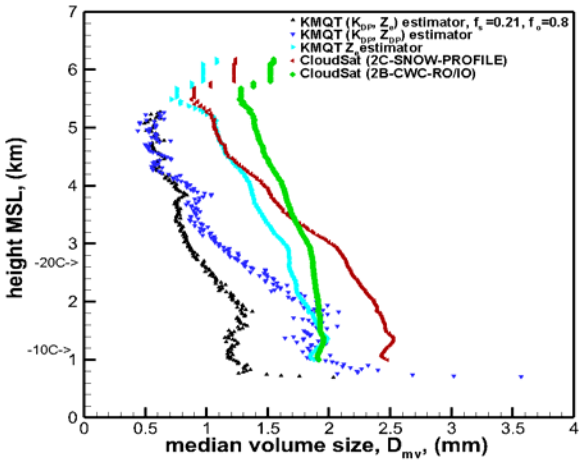

FIG.9. *Closely matched retrievals of particle median volume size from CloudSat 2C-SNOW-PROFILE (red) and 2B-CWC-RO/IO (green) algorithms and from KMQT based retrievals on 30 January 2014 (1903 UTC). Polarimetric KMQT retrievals are derived using QVPs. The KMQT reflectivity based estimates (cyan) are in a plane of the CloudSat cross section.*

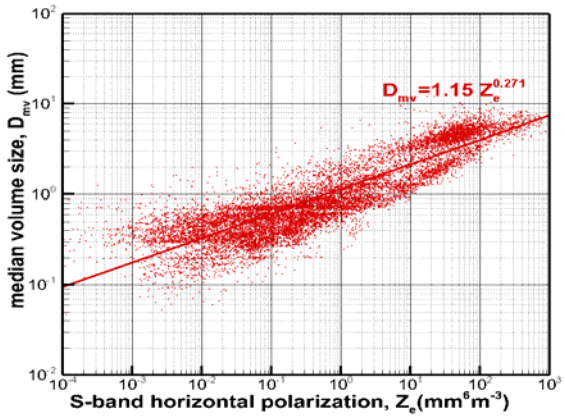

FIG.10. *A D_{mv} – S-band reflectivity* relation based on ISDAC data*. Reflectivity calculations assumed particle aspect ratio of 0.6 and a mass-size relation $m=0.0053D^{2.1}$ (cgs units).*

2C-SNOW-PROFILE retrievals provide the smallest values of IWC and the difference between the estimates from the two CloudSat standard retrievals is between factors of 2 and 3. Polarimetric KMQT estimates are in a relatively close agreement with CloudSat IWC - reflectivity regression based ice content retrievals. Ground-based size retrievals obtained using the IWC-Z_e – temperature statistical regressions show very little variability with height, which is likely due to not very adequate accounting for the temperature dependence of the regression coefficients.

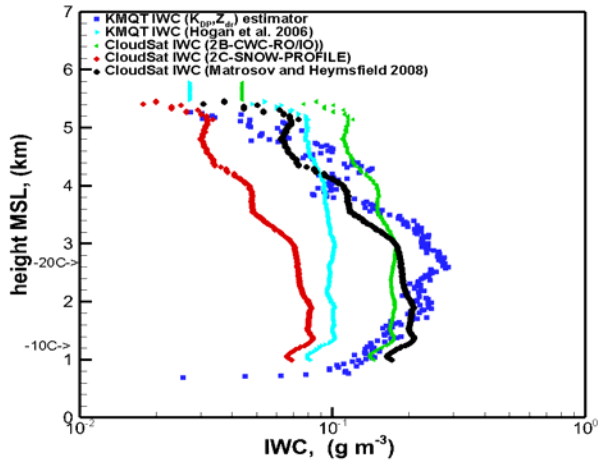

FIG.11. *Closely matched IWC retrievals from CloudSat 2C-SNOW-PROFILE (red), 2B-CWC-RO/IO (green), Matrosov and Heymsfield (2008)(black) algorithms and from KMQT polarimetric (blue) and regression (cyan) based retrievals on 30 January 2014 (1903 UTC).*

4. CONCLUSIONS

Ground-based and CloudSat radar retrievals of precipitating ice microphysics were closely collocated in space and time during satellite overpasses over operational (S-band) weather and research cloud radar sites during precipitating ice events. The differences in the fields of view of different radars and attenuation effects were approximately accounted for.

Different types of ice hydrometeor size retrievals were expressed in terms of median volume particle size, D_{mv}, for meaningful intercomparisons. These intercomparisons of matched retrievals revealed that estimates from various algorithms provide results which differed by as much as factor of 3. Size retrievals based on polarimetric radar measurements are, on average, smaller than regression-based retrievals from reflectivity measurements. Polarimetric retrievals at S-band are generally available when the specific differential phase is greater than about 0.05 deg km^{-1}. Significant differences in characteristic particle size retrievals were present even for the results from two different standard CloudSat algorithms (i.e., 2C-SNOW-PROFILE and 2B-CWC-RO/IO algorithms), which use the same measurements. This suggests existence of a relatively high uncertainty of retrievals. Given this uncertainty, a simple approach based on statistical relations between D_{mv} and observed radar reflectivity provides meaningful results.

Intercomparisons of matched ice water content retrievals also indicated substantial differences in the results from different algorithms. The corresponding differences between various retrievals were comparable with those for characteristic ice hydrometeor size. Comparisons of matched W-band reflectivities from the well calibrated CloudSat CPR and the DOE ARM Oliktok Point scanning cloud radar indicated that the SACR absolute calibration was good to within about ± 2 dB.

REFERENCES

Hogan, R.J., M.P. Mittermaier, and A.J. Illingworth, 2006: The retrieval of ice water content from radar reflectivity factor and temperature and its use in evaluating a mesoscale model. *J. Appl. Meteor. Climatol*., **45**, 301-317.

Maahn, M., U. Loenert, P. Kollias, R.C. Jackson, and G.M. McFarquhar, 2015: Developing and evaluating ice cloud parameterizations for forward modeling of radar moments using in situ aircraft observations. *J. Atmos. Oceanic Technol. 32, 880-903.* DOI:10.1175/JTECH-D-14-00112.1

Matrosov, S.Y., 2019: Comparative evaluation of snowfall retrievals from the CloudSat W-band radar using ground-based weather radars. *J. Atmos. Oceanic Technol*. **36**, 101-111. doi:10.1175/JTECH-D-18-0069.1.

Matrosov, S.Y., and A.J. Heymsfield, 2008: Estimating ice content and extinction in precipitating cloud systems from CloudSat radar measurements. *J. Geophys. Res*., **113**, D00A05, doi: 10.1029/2007JD009633

Matrosov, S.Y., and A. Battaglia, 2009: Influence of multiple scattering on CloudSat measurements in snow: A model study. *Geophys. Res. Lett*., **36**, L12806, doi:10.1029/2009GL038704

Matrosov, S.Y., and A.J. Heymsfield, 2017: Empirical relations between size parameters of ice hydrometeor populations and radar reflectivity. *J. Appl. Meteor. Climatol*., **56**, 2479-2488. DOI: 10.1175.JAMC-17-0076.1

Matrosov, S.Y., G.G. Mace, R. Marchand, M.D. Shupe, A.N. Hallar, I.B. McCubbin, 2012: Observations of ice crystal habits with a scanning polarimetric W-band radar at slant linear depolarization ratio mode. *J. Atmos. Oceanic Technol.,* **29**, 989-1008. DOI: 10.1175/JTECH-D-1100131.1

Ryzhkov, A.V., P. Bukovcic, A. Murphy, P. Zhang, and G. McFarquhar, 2018: Ice microphysical retrievals using polarimetric radar data. *Proc. 10th European Conference on radar in meteorology and hydrology* (ERAD 2018), 494-504. https://library.wur.nl/WebQuery/wurpubs/539463

Sassen, K., S.Y. Matrosov, and J. Campbell, 2007: An attenuation-driven upside-down lidar analog, *Geophys. Res. Lett*., **34**, L16818, doi:10.1029/2007GL030291

Shupe, M.D., T. Uttal, and S.Y. Matrosov, 2005: Arctic cloud microphysics retrievals from surface-based remote sensors at SHEBA. *J. Appl. Meteor.*, **44**, 1544-1561.